Proceedings of Global Power and Propulsion Society
ISSN-Nr: ???
GPPS Chania22
12th–14th September, 2022

www.gpps.global

GPPS-TC-2022-97

Inclined Slot Cooling of the Pressure Side Rims of Squealer Tips

Joao A C Vieira
University of Oxford
joao.vieira@stcatz.ox.ac.uk
Oxford, Oxfordshire, United Kingdom

John Coull
University of Oxford
john.coull@eng.ox.ac.uk
Oxford, Oxfordshire, United Kingdom

Peter Ireland
University of Oxford
peter.ireland@eng.ox.ac.uk
Oxford, Oxfordshire, United Kingdom

ABSTRACT

The blade tip is a particularly critical component of the high pressure turbine because the hot gas leaking over it causes a loss of efficiency and degrades the blade. This tip degradation is often a limiting factor of engine life. Squealer designs tend to have high efficiency, but the pressure side rims are particularly vulnerable due to their large surface area and the difficulties of shielding them from hot overtip leakage flow.

This paper considers a new approach to cooling the pressure side rim using an inclined slot inside a recessed step. Compared to conventional cooling strategies, in which coolant is provided by multiple cylindrical holes, the slot feature improves cooling effectiveness by more than 50% in key regions of the pressure side rim, whilst also allowing reduction in coolant mass flow. The concept design is developed using a combination of Computational Fluid Dynamics (CFD) calculations and experiments on a linear cascade with representative Mach and Reynolds numbers.

1 INTRODUCTION

A clearance gap must be maintained between the tips of rotating turbine blades and the stationary casing. For un-shrouded designs, an Over-Tip Leakage (OTL) flow is driven through this gap by the pressure difference across the blade (Denton, 1993). OTL flows generate significant loss of aerodynamic efficiency throughout gas turbines, for this reason squealer tips are often employed to reduce the leakage mass flow and loss. In the High-Pressure (HP) turbine, hot leakage flow can also degrade the blade tip, limiting engine life (Bunker, 2004). With the need for ever-increasing thermal efficiency and turbine entry temperatures (Dutta et al., 2000), it is becoming increasingly difficult to sufficiently cool the HP blade tip, particularly the pressure side rims and the thin Trailing Edge (TE) regions (Bunker, 2004). The aim of the current work is to substantially improve the cooling effectiveness in this region.

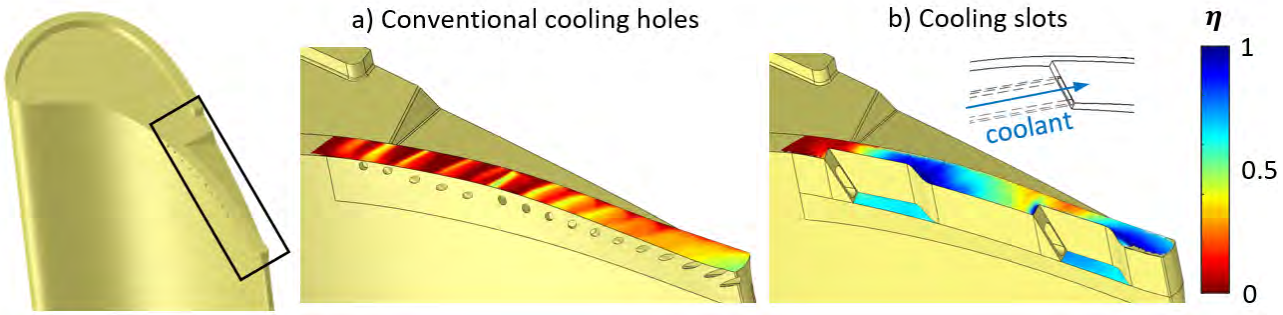

Figure 1: Experimental film cooling effectiveness contours overlapped over CAD renders of the tested high-pressure turbine tips. a) is a baseline tip with conventional cooling holes and b) is a test tip with two inclined cooling slots using 9% less coolant.

This work is licensed under **Attribution 4.0 International (CC BY 4.0)**
See: https://creativecommons.org/licenses/by/4.0/legalcode

1.1 Conventional Cooling with Discrete Holes

The most common means to provide cooling to the PS rim is to use a series of discrete holes distributed along the external pressure surface of the blade. Numerous examples are given in Kwak and Ahn (2003), Bunker (2004), Ahn et al. (2005), Hofer and Arts (2009), Zhang et al. (2011), O'Dowd et al. (2013) and Saul et al. (2019). The conventional cooling approach shown in Figure 1.a is used as a baseline for the current study. As can be seen from the measurements of cooling effectiveness η (detailed below), the top of the rim is reasonably well-cooled at the blade trailing edge (η ~0.3), but further upstream the cooling is intermittent. Thus, there is a need to achieve more effective cooling in this region.

1.2 Slot Cooling

It has been demonstrated for some time that slot cooling can achieve higher effectiveness than discrete holes for film cooling on blade sections (Cunha and Chyu, 2006). In practice, their use on aerofoil sections has been limited because of the stress limitations. Slots have however been used to cool aerofoil TE sections. Yang and Hu (2012) experimentally examined the aerothermal of a rectangular slot geometry, focusing on the detailed measurement of the flow field via particle image velocimetry and correlating the identified features to the measured FCE. Further work on TE slot cooling includes that of Niharika et al. (2016) and Wong et al. (2016).

Slot cooling has also been applied to blade tips, but in general only for cooling the interior cavity of squealer tips. Zhang et al. (2022) examined slots with radially-outward flow, distributed across the tip cavities in a cascade. Zhang et al. (2021) introduced streamwise slots into their cavity by integrating them into ribs inside the cavity. Neither of these examples targeted the pressure surface rim.

1.3 Squealer Shelf Cooling

Another approach that has been seen in the patent literature, and some engines, is to cut a small shelf into the length of the PS rim and provide coolant using discrete radially-aligned holes (Cherry et al. (2002), Leeke et al. (2003) and Correia et al. (2008)). In general these approaches are believed to be beneficial because some portion of the coolant is trapped in the separation bubble generated as the OTL flow separates from the shelf edge. Further examples include the shelf at the TE of PS rim given in Crites et al. (2013). Another approach is shown in Lee et al. (1998), where a trench is cut into the tip of the squealer rim and fed with discrete cooling holes. The current study suggests that the inclined slots developed in this paper achieve significantly higher cooling effectiveness than these existing shelf designs.

1.4 Concept: Inclined Slots With Steps

This paper develops a cooling concept which is shown in Figure 1.b, and consists of a step on the Pressure Side (PS) rim of the blade tip with an inclined protrusion containing a cooling slot. With respect to previous designs, the key features to note are:

1. The design specifically targets the exterior of the squealer rim, rather than the cavity interior or blade TE (as in the previous slot studies).
2. The slot does not inject flow radially, but is inclined in a largely streamwise direction. This is crucial to achieving a high area of coolant coverage. The streamwise momentum of the injected coolant causes coolant to follow along the length of the rim, rather than simply being drawn over the blade tip.
3. The slot is recessed into the blade by means of an inclined step cut into the squealer rim, rather than an axial shelf.

1.5 Aims, Approach and Paper Outline

The key aims of this paper are to develop the inclined slot concept, to understand the flow behaviour and to quantify its performance compared to conventional cooling designs.

To this end, the paper uses a Computational Fluid Dynamics (CFD) study to rapidly explore the design space and understand the sensitivities. To provide greater confidence, the most promising designs were tested experimentally on a transonic cascade representative of HP turbines, which demonstrates a significant cooling effectiveness improvement.

The paper is organised as follows. Section 2 describes the key slot geometry parameters. Section 3 describes the experimental and CFD methods. Section 4 uses CFD to explore the design space, and the experiments are presented in Section 5. The data are complemented in Section 6 by simulating the impact of additional engine-representative conditions.

2 DESIGN PARAMETERS

Figure 2.b shows an inclined slot applied to a squealer tip; the cavity of this tip is open towards the trailing edge, but this feature is inconsequential for the slot performance (the inclined slot can also be applied to solid tips, i.e. without a cavity or rims). The slot exit is placed on an inclined step surface cut into the rim of the pressure surface, at around mid-chord in this design. A shelf cut into the pressure surface extends downstream of the slot and blends smoothly back into the blade. The following design parameters control the size and position of the key features.

The slot and inclined step surface can be characterised as shown in Figure 2.a. The distance from the bottom of the shelf (h) and the offset from the external edge (d_{wall}) were set to be 0.5% and 0.4% of axial chord (C_{ax}) respectively to allow clearance for manufacturing. The width (w) of the recessed step was set to 50% of the total rim width for all studied geometries. The length (l) and diameter of the slot (d_n) together control the slot aspect ratio and area. The influence of area is studied in detail in Section 4.3. For fixed mass flow, reducing slot area increases the Blowing Ratio (BR), thus increasing

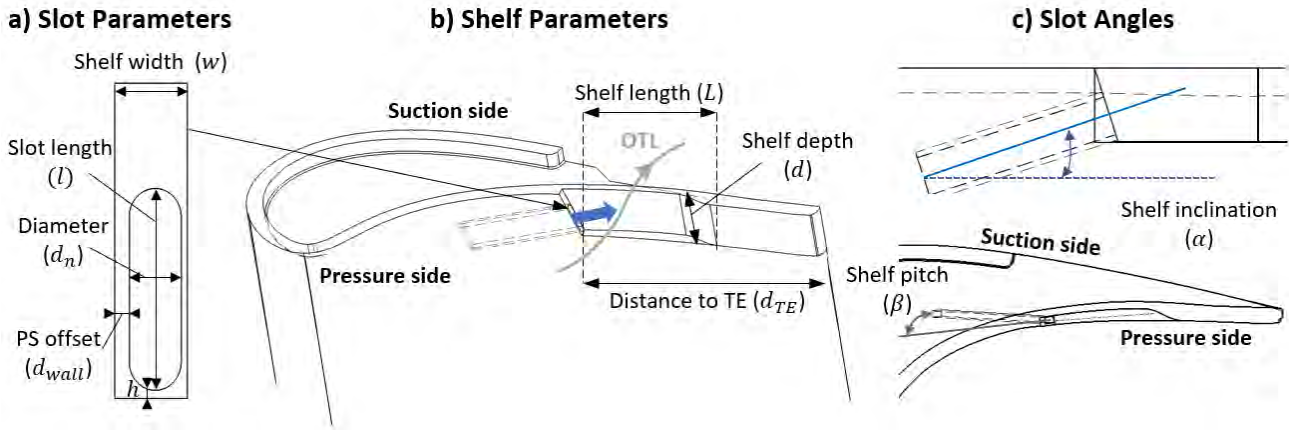

Figure 2: Schematic of the dedicated pressure side rim cooling slot depicting the parametrisation of its main features: a recessed PS shelf and an inclined cooling slot.

the streamwise momentum and spread of the coolant. Meanwhile, the higher flow gradients cause more mixing and tend to reduce effectiveness. Similar trade-offs are observed for fixed geometry with varying coolant flow rate.

The shelf length and height can be parametrized by three variables (Figure 2.b). Longer shelf lengths (L) have a larger impact on the blade geometry, but improve manufacturability by improving drill access for the slot. Depth (d) sets the position of the shelf in the spanwise direction. Together with the slot parameters, d sets the spanwise height of the slot which can alter the trajectory of the cooling jet. The distance (d_{TE}) controls the streamwise position of the shelf and slot.

The coolant ejection direction of the slot (Figure 2.c) is defined by two angles: the vertical angle between the inclined surface and the shelf (α) and the pitch angle into the blade (β). Of the two, α has the largest impact on performance, since it defines the angle at which the coolant flow approaches the rim (see Section 4.4). Optimal coverage occurs at lower values of α and β, which diminishes the skew between the direction of the cooling jets and that of the PS rim. These angles will also be limited by manufacturing constraints.

3 METHODS

The test vehicle for examining the slot concept is the High Speed Linear Cascade (HSLC) rig, designed to evaluate the aerothermal performance of HP turbine blade tips. The Computational Fluid Dynamics (CFD) calculations are largely performed for the experimental conditions, but additional calculations are used to simulate effects that cannot be modelled in the cascade, namely coolant density and the relative motion of the casing (Section 6).

3.1 Experimental Setup

The HSLC is a 5-blade cascade with variable tip gap, which runs in blowdown mode with around 90 second run time (Vieira et al., 2021). The experiments are run at transonic exit Mach number (0.99) and a Reynolds number of 1.24×10^6. Further details can be found in Zhang et al. (2011) and O'Dowd et al. (2013).

Film cooling is delivered to the blade tips using dedicated cooling feeds. Cooling effectiveness distributions are measured using dual-component Pressure Sensitive Paint (PSP). This optical measurement method employs a mass transfer analogy to obtain adiabatic film cooling effectiveness. The calculation evaluates the phosphorescent excitation of the PSP coat applied to the test pieces, the emissivity of which is dependent on the local partial pressure of Oxygen. This property is exploited to calculate local partial pressures using a filtered color-corrected camera (Han and Rallabandi, 2010). For each measurement, ambient temperature Air and Nitrogen are sequentially used as coolant to generate a comparative evaluation, in which Nitrogen functions as an effective tracer gas for the distribution of coolant over the surface of the blade. This setup gives a near-unity density ratio between the mainstream flow and the cooling jet. Dual-component PSP includes a second, temperature-dependent paint that allows one to correct for temperature variations in the paint response, which leads to greater accuracy in the calculated effectiveness. Linear perturbation analysis demonstrates that the experimental uncertainties depend on the signal level, giving local uncertainties of approximately $\pm$ 0.045 for $\eta < 0.2$ and $\pm$ 0.015 for $0.2 < \eta < 1.0$, at a 95% confidence level.

Though not the focus of this paper, aerodynamic loss measurements are performed 0.5 C_{ax} downstream of the cascade trailing edge using a 4-hole probe with 1.2 mm head diameter. Traverses are performed on a grid of 26 pitchwise locations by 10 spanwise locations. Total pitchwise length is one blade pitch, while spanwise length is 25% of blade span. Uncertainty values are: $\pm0.31°$ in yaw angle, $\pm0.50°$ in pitch angle, ±0.014 in Mach number and $\pm0.96\%$ in stagnation pressure (Vieira et al., 2021).

3.2 Meshing and CFD

To model the cascade, a single periodic passage is simulated, with the inlet plane located two axial chords upstream of the blade Leading Edge (LE) and the outlet one axial chord downstream of the TE. A distribution of total pressure matching the cascade is specified at the inlet, together with constant total temperature and flow angle. The slot inlet feed is setup as a constant mass inflow, with fixed inlet angles and temperature. A constant static pressure was specified at the outlet. The hub, casing and the entirety of the blade are no-slip walls.

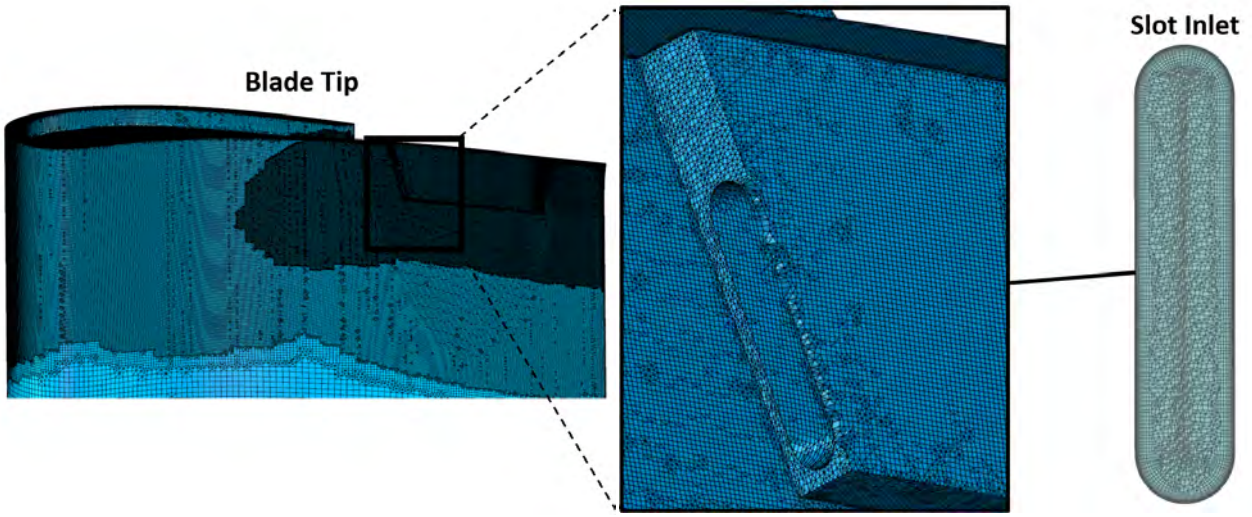

Figure 3: Details of the numerical mesh for an example inclined slot geometry.

An unstructured mesh (Figure 3) was generated using BoxerMesh version 3.8.3, combining an octree freestream mesh with body-fitted viscous layers. Surface y^* values in the order of 0.5 were obtained for the entirety of the tip region. The mesh resolution at the tip is particularly high, with a refinement focus in the region downstream of the slot, which is the principal area of interest for the study. Total mesh size depends on the geometry, but is typically between 20 and 22 million nodes, in accordance to the mesh independence study (Section 3.4).

Reynolds-Averaged-Navier-Stokes (RANS) calculations are performed using the Rolls-Royce in-house Hydra solver (Moinier, 1999). Spatial discretisation is performed with a 2^{nd} order upwind edge-based finite volume method and time stepping employs a 5^{th} order Runge-Kutta explicit scheme with Jacobi preconditioning. The turbulence model used in this study was the k-ω with Shear-Stress Transport scheme (Menter, 1994).

3.3 Film Cooling Effectiveness Calculation and Associated Performance Metrics

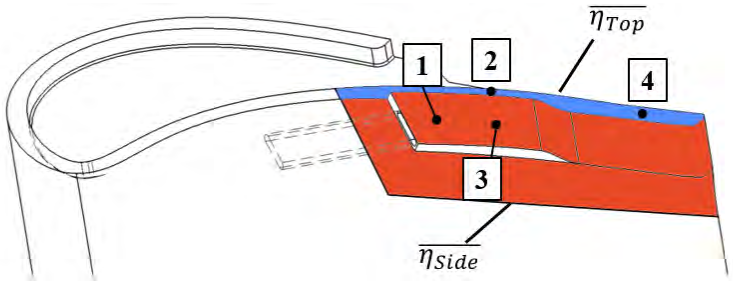

Figure 4: Averaging regions for the cooling evaluation parameters. Numbered positions are the probing points implemented in the mesh independence study.

To mimick the rig setup (Section 3.1), most of the calculations use coolant with almost the same temperature as the mainstream flow. A two temperature approach was used to calculate the surface FCE of the CFD simulations, by comparing the surface temperature data of two simulations with coolant temperatures set 10 degrees apart:

$$\eta = \frac{T_{ref} - T_{test}}{T_g - T_c} \tag{1}$$

Where T_g and T_c are the total temperatures of the mainstream (285 K) and of the coolant (275 K), respectively. The blade tip surface temperatures of the "reference" case (T_{ref}) represent the nominal condition with the coolant inlet set to the same temperature as the mainstream (285 K), whilst the temperatures in the cooled "test" simulation (T_{test}) portray the impact of the coolant stream, with the coolant set to 275 K.

While the pointwise η over the surface of the tips is an useful comparison metric on its own, it is also useful to establish the following integrated parameters defined in Figure 4:

- $\overline{\eta_{top}}$: spatial-averaged η over the top surface of the PS rim, between 60% and 100% axial chord (C_{ax}).

- $\overline{\eta_{side}}$: spatial-averaged η over the side surface of the PS rim. Averaging region is, again, between 60% and 100% C_{ax} in the axial direction and between 90% and 100% of blade span.
- $\overline{\eta_{av}}$: area-based weighted average of $\overline{\eta_{top}}$ and $\overline{\eta_{side}}$.

Figure 4 color-codes top and side averaging regions on an example geometry. These are the key regions of the PS rim that the dedicated slot concept aims to cool in lieu of conventional cooling holes.

3.4 Mesh Sensitivity

Mesh independence was evaluated on a single case. A total of five meshes with identical mesh refinement settings but increasing grid density were examined, ranging from 7.4 to 39 million nodes.

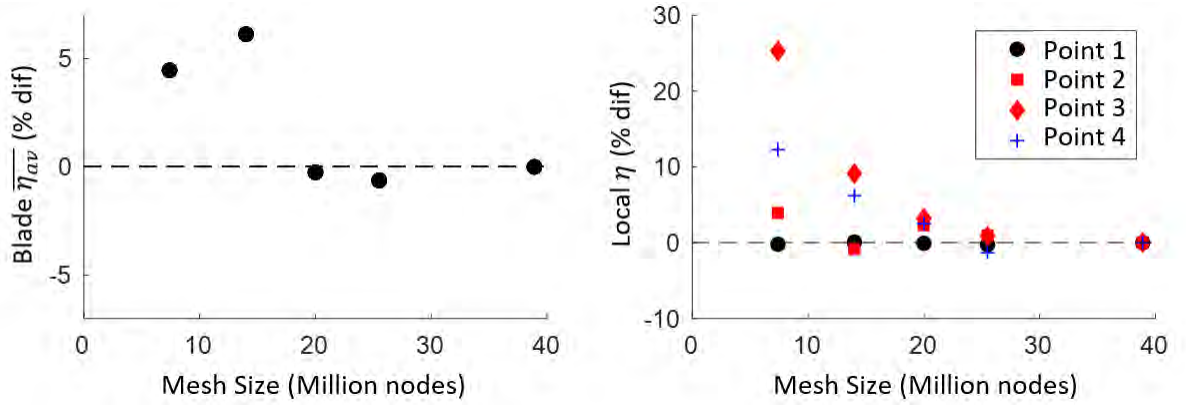

Figure 5: Percentage deviation of the mesh independence criteria from the values obtained at the highest density grid, plotted against number of nodes.

Grid sensitivity is assessed by considering area-averaged FCE over the two regions denoted in Figure 4, and by considering local FCE at four points downstream of the slot exit. The locations of these points (Figure 4) were strategically chosen to include (1) the saturated η region inside the recessed shelf; (2) a transition from high to low η at the top of the rim, in a region of high coolant dissipation; (3) a similar transition at the side of the rim and (4) a location downstream of the main area of effectiveness of the slot, where η is lower.

The data in Figure 5 evidences that suitable convergence occurs at mesh sizes of 20 million nodes, where the variation in global FCE is only 0.25% compared to the case with the highest mesh density. Expectedly, larger variations are observed in the localised FCE data present in high-dissipation regions, which is the case for points 2, 3 and 4. Nevertheless, the η values at these points converge convincingly with the increase of mesh density. Accordingly, the meshes for all the CFD cases in this publication were generated with the same refinement settings as the 20 million node grid.

4 EXPLORING THE DESIGN SPACE

The performance of the inclined slot concept is first studied in CFD. An initial "nominal" slot design is first described, before the overall performance of some key designs are assessed. The design sensitivities and dual-slot configurations are then explored. The range of design parameters for each case are given in Table 1, which will be referenced throughout this section.

4.1 Nominal Slot Design Behaviour

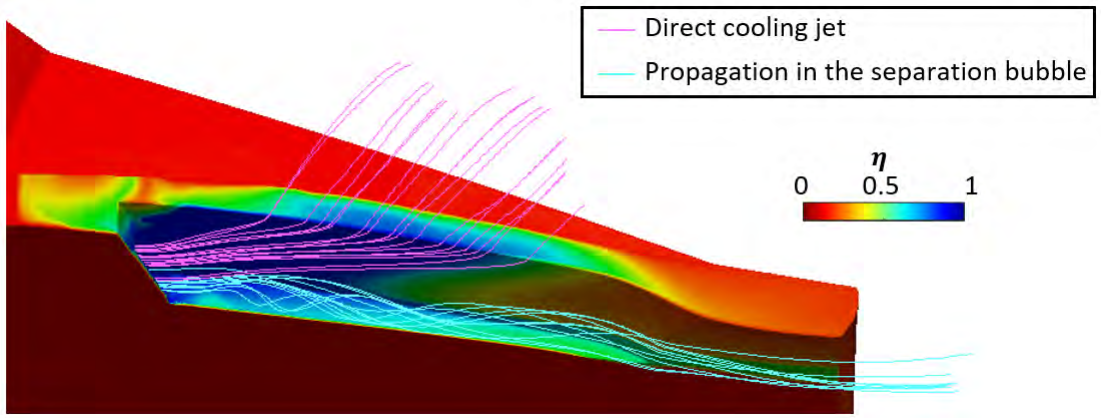

Figure 6: Film cooling effectiveness contour of the single cooling slot geometry at nominal conditions with superimposed streamlines showing the two modes of coolant propagation.

Figure 6 shows the nominal single slot case at a tip gap size of 1.15% g/S - where the tip gap (g) is defined as the

distance between the top surface of the rims and the casing, which is non-dimensionalised by the blade span (S) - and a non-dimensionalised mass flow rate (mi_R) of 45% (i.e. 45% of the baseline conventional design), demonstrating the basic behaviour of the dedicated slot feature. In general, the coolant ejected from the inclined slot has a much higher streamwise momentum than the local mainstream flow, which tends to pass almost straight over the tip at this location. As a result, the coolant tends to propagate along the tip, cooling a larger area.

It is seen that most of the coolant follows the ejection direction of the slot for some distance, before being drawn over the top of the PS rim (pink streamlines in the figure). This behaviour provides relatively high η values for a section of the rim roughly equal to the shelf length in the case with nominal slot flow area. After the high effectiveness region, the strong OTL flow causes the coolant to dissipate, which results in relatively low film effectiveness downstream of the shelf. Figure 6 also shows that some coolant seeps into the separation region created by the shelf, where it propagates along the pressure surface to the blade trailing edge (blue streamlines). This second coolant flow path further increases the cooled area and the average effectiveness.

4.2 Snapshot of Overall Performance

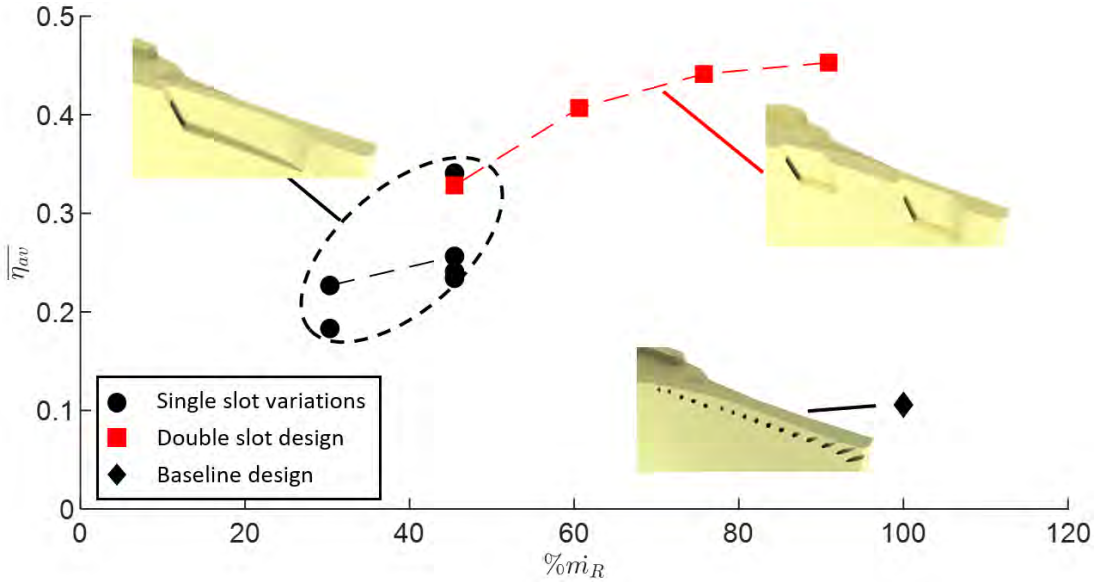

Figure 7: Performance metric $\overline{\eta_{av}}$ plotted against total coolant mass flow for CFD cases with 1.15% g/S tip gap size. Single slot geometries are shown as circles, dual slot design as squares and the baseline tip as a diamond.

The overall performance of various slot designs are compared to the conventional cooling design from Figure 1.a. Figure 7 charts the average film effectiveness in the target region, $\overline{\eta_{av}}$ (see Section 3.3), against the non-dimensionalised mass flow rate. The circles show single slot configurations, the diamond markers are the baseline reference values and the dashed lines link cases that were examined at multiple coolant mass flow rates. The square symbols indicate the dual slot design, discussed in detail in Section 4.5. The conventional baseline tip is on the bottom-right, having the lowest $\overline{\eta_{av}}$ value (0.11) and the highest coolant expenditure. On the left, the range of single slot variants are distributed between $\overline{\eta_{av}}$ values of 0.18 and 0.34. The dual slot geometry matches the highest performing single slot cases at $mi_R = 45\%$ and then proceeds to significantly improve upon that as the coolant mass flow increases, with the $mi_R = 91\%$ case having the highest $\overline{\eta_{av}}$ of the studied cases, at a value of 0.45.

The following two subsections will examine the impact of key slot design parameters on the cooling performance of the single slot design, arranged from highest to lowest relative importance: slot flow area (4.3) and slot angles (4.4). Dual slot designs are then discussed in Section 4.5. Table 1 shows the parametrisation of the test geometries for each study.

4.3 Sensitivity to slot flow area

The first case study is that of the slot coolant ejection area. The slot flow area is defined by the slot length (l) and nominal diameter (d_n) (Figure 2.a). As shown in the first row of Table 1, d_n was kept constant at 1.6% C_{ax}, while l was varied between 5.5 and 11.1% C_{ax} to give a +/-33% variation in area from the nominal slot design. The three cases were simulated at a tip gap size of 1.15% g/S.

Figure 8 charts the average effectiveness values on the top and side surfaces against the coolant ejection area. Black markers refer to $\overline{\eta_{top}}$ and red markers to $\overline{\eta_{side}}$, while the diamond markers are reference values for the baseline tip. The relationship between coolant coverage and slot BR is evidenced in the slot data (circle markers) where it is seen that both averages peak at nominal slot flow area ($A_i = 1$).

	Cases	l/C_{ax}	α	β	d_n/C_{ax}	L/C_{ax}	d/C_{ax}	w/C_{ax}	d_{TE}/C_{ax}
Slot Area Study	Smaller slot area	5.5%	18°	8°	1.6%	36.0%	12.2%	2.0%	50.0%
	Nominal case	8.3%							
	Larger slot area	11.1%							
α **Study**	Angle α case 1	8.3%	4°	8°	1.6%	36.0%	12.2%	2.0%	50.0%
	Angle α case 2		30°						
	Angle α case 3		45°						
β **Study**	Angle β case 1	8.3%	18°	0°	1.6%	36.0%	12.2%	2.0%	50.0%
	Angle β case 2			16°					
Double Slot Study	Fwr. Slot / Aft. Slot	8.3%	18°	8°	1.6%	20.0%	12.2%	2.0%	62% / 24%

Table 1: Parameters of the geometries involved in the study of the inclined slot concept.

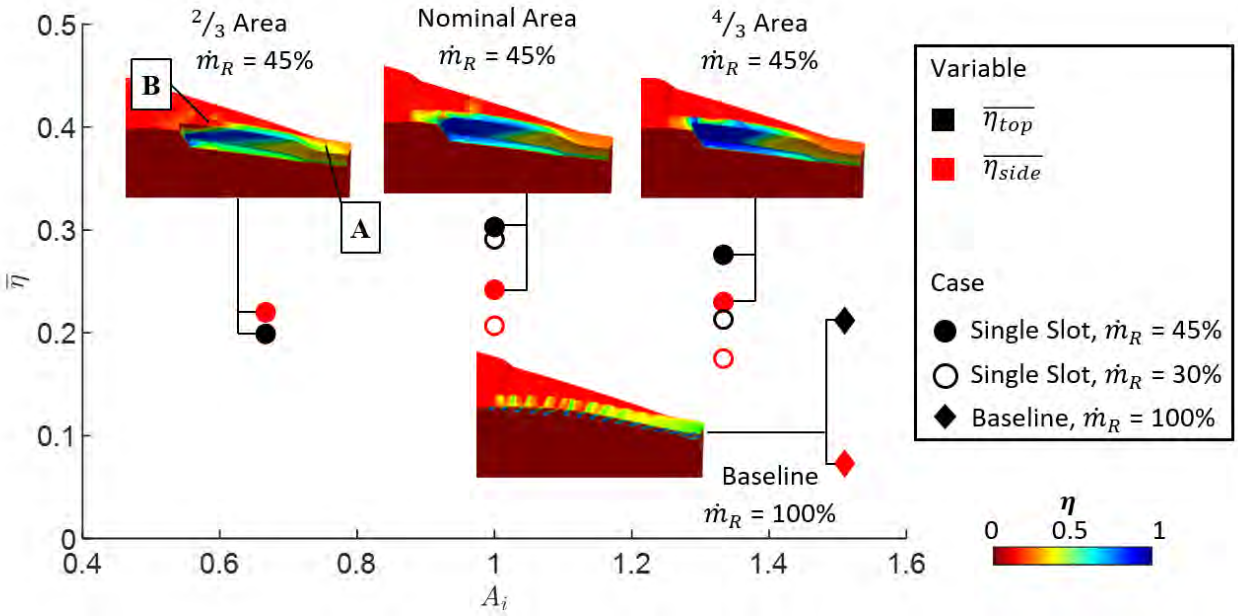

Figure 8: Area-averaged η_{top} and η_{side} for the cases with varying slot flow area (A_i). Single slot cases shown as circles and the reference values for the baseline tip as diamonds.

Slot blowing ratio is defined as:

$$BR = \frac{\rho_c V_c}{\rho_m V_m} \tag{2}$$

Where the numerator refers to the velocity and density of the coolant, whilst the denominator refers to the mainstream gas. Thus, for a fixed mass flow rate, decreasing the slot flow area, increases jet velocity and causes the slot BR to increase, whilst the reverse occurs when the slot area is increased. The effects of decreasing slot area can be seen in the $2/3\ A_i$ case (leftmost insert plot). The smaller area increases the blowing ratio of the slot, causing the coolant to be projected further along the PS rim, at the detriment of effectiveness in the near-slot region. This change leads to an increase of η_{top} in the latter 10% C_{ax} of the rim (label A in the figure), but significantly lowers the values in the 60 to 85% C_{ax} region (label B). In addition, the higher velocity jet undergoes greater dissipation, lowering average η values. A similar effect occurs on the side of the rim, where this case achieves slightly more coverage after the 80% C_{ax} point, while having lower upstream values.

Inversely, the larger slot flow area case (rightmost insert plot) causes a decrease in slot BR, shifting the coolant coverage and associated peak η values upstream. This factor leads to a large improvement in near-slot η_{top}, but penalises η_{side} on the latter 20% C_{ax} of the rim. A similar effect is observed when BR is changed by varying mass flow rate for a given design (clear circle markers in Figure 8), which highlights the dependency of the coolant distribution on slot blowing ratio. It is also seen that the nominal flow area slot case is less affected by the decrease in coolant mass flow rate than the larger area case, which underwent a reduction of ~30% in both performance metrics. It is expected that this difference is largely due to the slot BR in each of the cases, which is more optimal with nominal slot area, resulting in jets that have a higher resilience to the change in coolant mass flow.

Overall, compared to the baseline tip (diamond markers in the figure), it is shown that the single slot geometries greatly outperform the reference conventional design in both $\overline{\eta_{top}}$ and $\overline{\eta_{side}}$ for most of the examined region, with the conventional tip only achieving superior η_{top} coverage at the last 10% C_{ax} of the rim. Average values for the nominal flow area case show a 44% improvement over the reference for $\overline{\eta_{top}}$ and of 250% for $\overline{\eta_{side}}$, with a coolant expenditure of less than half that of the reference case.

In conclusion, it is seen that the cooling performance of the dedicated slot geometry is highly dependent on slot blowing ratio, with the data suggesting that blowing ratio increases are less penalising to the overall performance than blowing ratio decreases. The data evidenced that, for this dedicated slot configuration at the identified optimal conditions, there is an optimal area of coverage consisting of roughly 20% C_{ax} downstream of the slot. This area can be increased by increasing slot blowing ratio, at the cost of having more diffuse coolant. Alternatively, one can also increase the number of slot features along the rim, which maximises both coverage and performance. This hypothesis is explored in Section 4.5.

4.4 Sensitivity to slot angles α and β

The orientation of the cooling slot in relation to the shelf plays an important role on jet direction and coolant propagation. This section details the study of the impact of the vertical angle α and the pitchwise angle β (Figure 2.c) on the cooling performance. In total, five variations to the baseline geometry were examined, three with incremental α angles: 4°, 30° and 45°; and two with incremental β angles: 0° and 16°, as shown in the middle two rows of Table 1. The lower α and upper β bounds of these distributions were established by the geometrical limitations of the underlying tip geometry, thus exploring the full range of allowable values. The nominal slot flow area case is also included as a sixth case, with the angles $\alpha = 18°$ and $\beta = 8°$. All cases were simulated at a tip gap size of 1.15% g/S and a coolant mass flow of $\dot{m}_R = 45\%$.

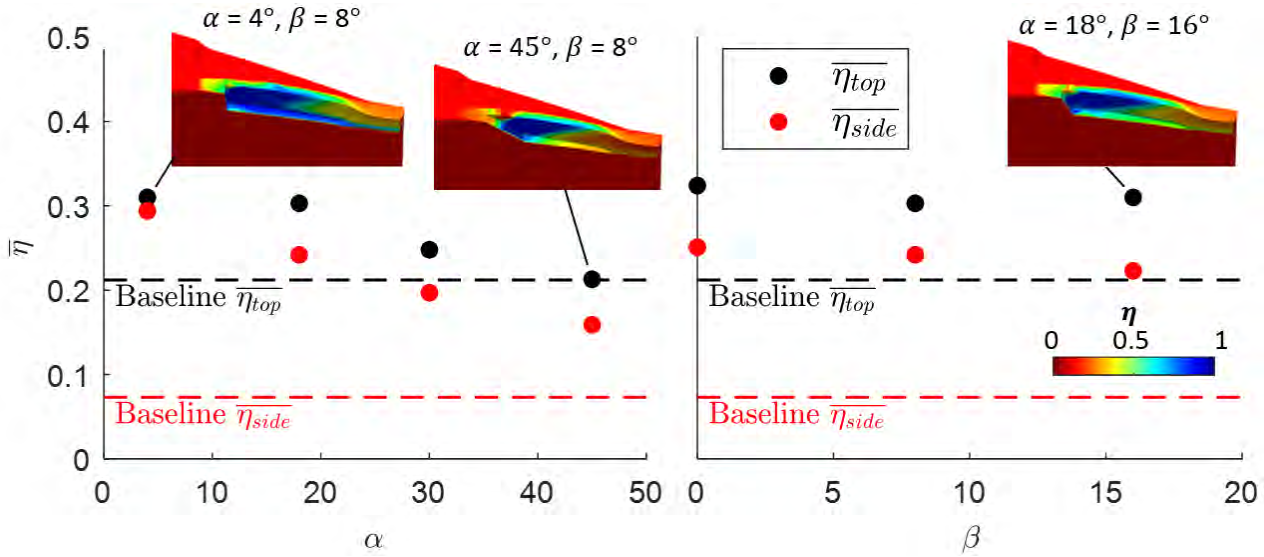

Figure 9: Area-averaged η_{top} and η_{side} for the cases with varying α and β slot angles. On the left, α data; on the right β data. Dashed lines are the reference values for the conventionally cooled baseline tip.

It is immediately apparent from the datapoints in the left-hand plot of Figure 9 that lower α angles improve: (1) the η magnitude on the top surface of the rim and (2) the overall coverage on the side surface. This increase in performance is expected, as lower α angles improve the alignment of the cooling jet with the shelf, which allows the jet to more effectively fill the shelf and enhances the shielding of the coolant against the dissipative action of the OTL flow. Additionally, the larger amount of coolant inside the shelf is greatly beneficial to η_{side}, as it not only improves the coverage on the side rim surface inside the shelf, but also increases downstream propagation along the side of the blade (Figure 6). In overall terms, this behaviour results in an essentially linear decrease of $\overline{\eta_{side}}$ with the angle α, as is shown by the red circular markers in Figure 9.

The impact of α on the top surface is more subtle. Black markers in the figure show that the most significant change occurs between the 30° and 45° cases, where the extreme slot inclinations cause the coolant to be mostly convected directly into the tip gap rather than propagating along the rim, considerably reducing coverage. Contrastingly, the two other α cases are mostly identical, except for the near-slot region, with the difference between the $\alpha = 4°$ and the $\alpha = 18°$ cases being just 2.3%, which implies that reducing α below 20° has diminishing benefits on the coverage of the top of the rim.

Sensitivity to β is shown in the right-hand plot in Figure 9. The pitchwise angle has an overall smaller impact on cooling performance compared to α, partly due to the smaller feasible range of values (limited by blade thickness). The $\beta = 0°$ case achieves the highest performance values, as this is the condition in which the coolant stream is parallel to the shelf surface and, thus, can more easily propagate along the rim surfaces. As the β angle increases, the coolant flow is gradually redirected away from the blade and into the ascending OTL flow, decreasing the amount of coolant available inside the shelf. On the side surface, this change results in a consistent, albeit small, reduction of $\overline{\eta_{side}}$, with the $\beta = 16°$ having an

overall value 11% lower than the $\beta = 0°$ case. In contrast, the only major difference at the top rim surface is the near-slot region in the $\beta = 0°$ case, resulting in a 7% increase over the nominal conditions ($\beta = 8°$), which performs almost identically to the $\beta = 16°$ case. Designs with higher β values would be expected to have worse cooling performance, but these are impractical unless thicker blade profiles were to be adopted.

In summary, it was made apparent from these two studies that the dedicated PS slot geometry functions optimally at low slot α and β angles, so that the cooling jet is directed approximately parallel to the PS rim.

4.5 Dual slots

The single slot designs achieved promising results in relation to conventional cooling schemes and were shown to be capable of cooling a region of up to 20% downstream of the slot. As depicted in Figures 8 and 9, this effective range resulted in undesirably low coolant coverage on the last 10% C_{ax} section of the PS rim. Increasing blowing ratio can increase coverage far downstream of the slot, but this results in greater near-field mixing, leading to a substantial reduction in overall cooling performance.

A dual slot configuration can be adopted to achieve greater coverage with high FCE. As shown in Figure 7, the design consists of two smaller shelves - with lengths of 20% C_{ax} - distributed along the TE of the PS rim. Location-wise, the d_{TE} of the fwr. shelf is 62% C_{ax}, while for the aft. shelf it is 24% C_{ax}. All other parameters of the two features are the same as those of the single slot design with nominal area (last row in Table 1). This dual slot geometry was simulated at four coolant mass flows, split equally between the two cooling orifices: from $\dot{m}_R = 45\%$ to $\dot{m}_R = 91\%$ total coolant feed.

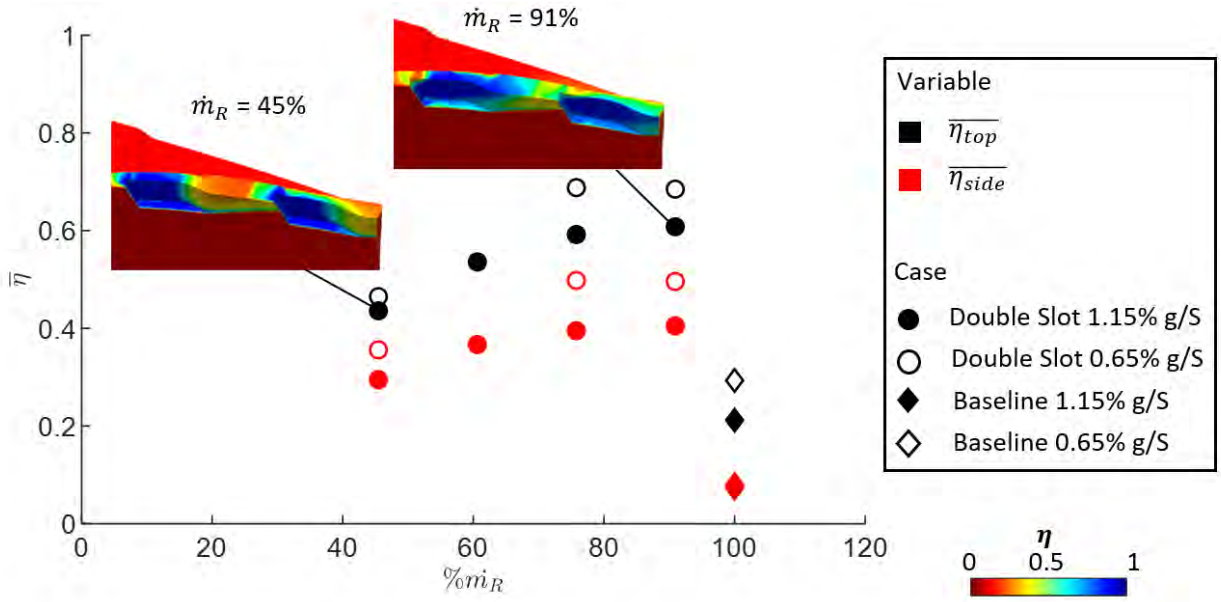

Figure 10: Area-averaged η_{top} and η_{side} for the double slot cases with varying coolant mass flow rate and tip gap size. Note that the y-axis limits differ from the previous $\overline{\eta}$ plots.

The η distributions are shown in the insert plots of Figure 10, a stark contrast exists between the dual slot and the single slot results (shown in Figures 8 and 9). There is a more complete cooling of the top of the rim, where the coverage provided by the fwr. slot is succeeded by that of the aft. slot, resulting in a substantially more consistent coverage of the target region of the rim. It should be noted that a low η patch is present between the shelves in the cases with lower $\dot{m}_R$, but it is completely eliminated in the cases with higher $\dot{m}_R$, as demonstrated in the right hand insert plot in Figure 10.

In regards to the general trends, data shows that increasing $\dot{m}_R$ is beneficial for the size and concentration of the coolant distribution on the downstream tip surfaces, causing a consistent increase in $\overline{\eta_{top}}$ and $\overline{\eta_{side}}$ up to $\dot{m}_R = 76\%$. However, little performance gains are present between the $\dot{m}_R = 76\%$ and $\dot{m}_R = 91\%$ cases, with an increase in performance metrics of only 2.5%, at the cost of 20% added coolant. These factors evidence a performance plateau of the dedicated PS slots, with the limiting coolant mass flow rate being roughly $\dot{m}_R = 45\%$ per slot at the tested conditions.

In comparison to the reference values of the baseline tip (diamond markers in the figure), the double slot $\dot{m}_R = 91\%$ case further develops on the benefits of the single slot configurations, achieving improvements of 185% and 455% over the $\overline{\eta_{top}}$ and $\overline{\eta_{side}}$ of the baseline tip, respectively, whilst using 9% less coolant. Moreover, since the performance of the $\dot{m}_R = 76\%$ case is similar to the of the $\dot{m}_R = 91\%$ case, it suggests that further coolant savings should be possible.

The impact of tip clearance was also examined in this study, with the clear circle markers representing the cases with smaller tip clearance (0.65% g/S). The data for the small tip gap cases show a substantial increase of $\overline{\eta_{top}}$ and $\overline{\eta_{side}}$, likely due to the smaller OTL mass flow causing less dissipation of the cooling jets and increasing overall coolant residency time. Thus, it is seen that the tip clearance reduction has a positive impact on the cooling performance of the dedicated PS slot over both rim surfaces.

In summary, the dual dedicated PS slot geometry demonstrates a substantial increase in cooling effectiveness over the conventional cooling schemes. The following section presents an experimental validation of this concept.

5 EXPERIMENTAL DEMONSTRATION OF THE DUAL SLOT DESIGN

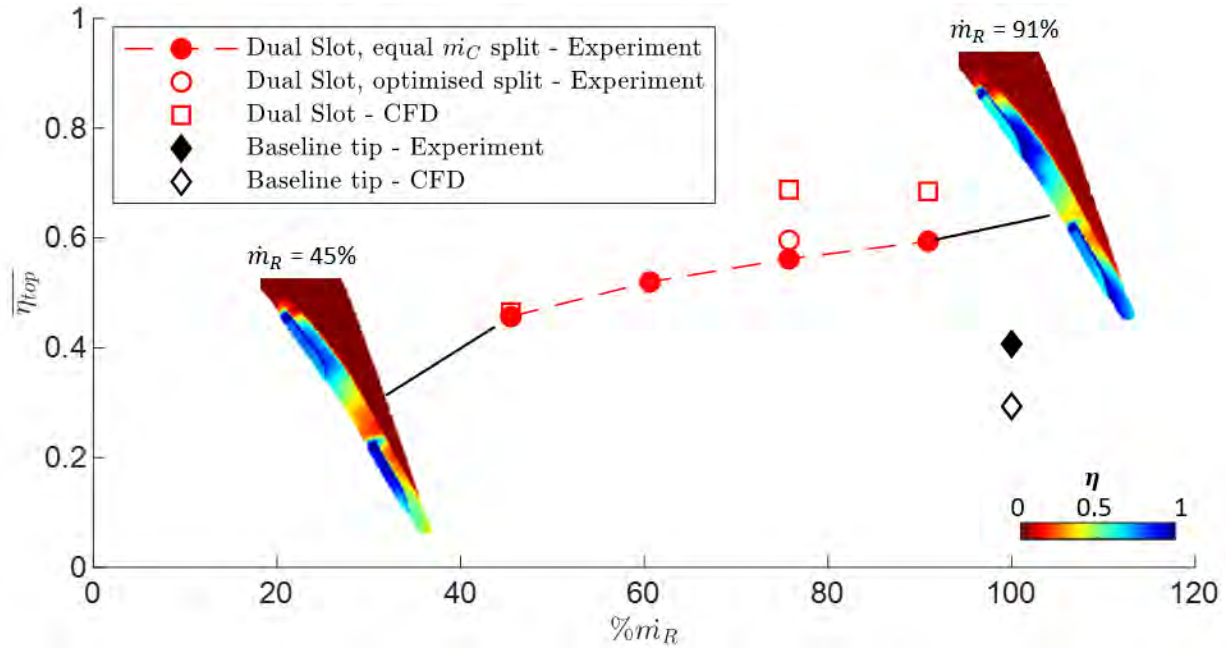

Figure 11: Plot of $\overline{\eta_{top}}$ experimental averages against coolant mass flow rate for the double slot and baseline tip geometries at small tip gap. Equivalent CFD data shown as red squares for the double slot design and as clear diamonds for the baseline.

The film cooling effectiveness of the dual slot design was measured on the HSLC at engine realistic Mach and Reynolds numbers using dual component PSP. The test tip was manufactured via stereolithography additive manufacturing using ABS plastic, with the rims edges and cooling orifices being machined to match the geometrical specifications. Test conditions for this geometry were the smaller tip gap setting (0.65% g/S) and the four coolant mass flow rates from the CFD study, which range from $\dot{m}_R$ = 45% to $\dot{m}_R$ = 91%, with the coolant being evenly spread between the slots. Results are shown in Figure 11. In addition, some optimisation of the coolant balance between the two slots was attempted, with the most successful case being a $\dot{m}_R$ = 76% configuration with a 3:2 split, resulting on 60% of the coolant being routed to the fwr. slot and the remaining 40% to the aft. slot (clear circle marker).

The η insert plots presented in the figure demonstrate that the excellent coolant coverage of the top rim surface generated by the dual slot design is successfully replicated in an experimental setting, corroborating the performance predicted in the CFD study. Impressively, the coolant distribution over the target TE portion of the rim is already exemplary in the $\dot{m}_R$ = 45% case (left insert plot) and improves further as additional coolant is added, with near perfect coverage of the rim being achieved in the $\dot{m}_R$ = 91% case (right insert plot).

In comparison to the experimental $\overline{\eta_{top}}$ value for the baseline tip at small tip gap, the dual slot design is shown to comfortably surpass the performance of the conventional cooling scheme throughout the trailing edge region of the rim, representing a coolant savings of 9% in the $\dot{m}_R$ = 91% case, while improving $\overline{\eta_{top}}$ by 46%. Optimising the split of coolant flow between the two slots maintained performance while saving approximately a quarter of the coolant mass flow rate. Additionally, optimisation of the individual slot geometries would provide even more benefit. Furthermore, the experimental data do not include the improvements on the side of the rim, where the CFD strongly predicts that the double slot configuration should greatly outperform the conventional cooling scheme. Thus, it is expected that the overall cooling advantage is greater than the value quoted above. The aerodynamic loss of the dual slot, as measured by the 4-hole probe, showed no significant differences in performance to that of the baseline tip, substantiating its position as the highest performing geometry.

In comparison to the CFD data from Section 4.5, the dual slot cases exhibited a $\overline{\eta_{top}}$ progression that is very similar to that predicted by the simulations. The red square markers in Figure 11 denote the CFD cases at the same tip clearance as the experimental data (0.65% g/S). As can be seen, CFD overpredicted the experimental effectiveness for the two higher $\dot{m}_R$ cases by approximately 20%, which is a relatively close agreement for RANS simulations.

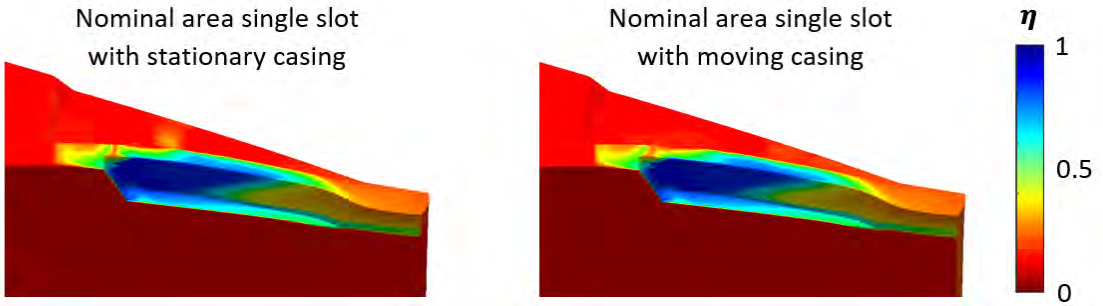

Figure 12: Film cooling effectiveness contours for the single slot geometry with flow nominal area and 1.15% g/S tip clearance. Case on the left has stationary casing, while the case on the right is setup with engine-representative casing motion.

6 SENSITIVITY TO REAL-ENGINE EFFECTS

6.1 Relative Casing Motion

The previously described simulations and experiments were realised in a purely stationary frame. To address the impact of rotor rotation on the cooling performance of the slot features, a version of the single slot geometry was simulated with engine-representative casing motion. This simulation was setup similar to those described in Section 3.2, except for the casing BC, which was set to move as a linear translation at engine-representative tangential velocity in the SS to PS direction .

Examination of the η distributions between the baseline in the stationary and rotating frames (Figure 12) does not reveal any major differences, with both $\overline{\eta_{top}}$ and $\overline{\eta_{side}}$ being within 1% of each other for the two cases. This resilience to the scraping flow is consistent with similar calculations performed by Virdi et al. (2015), Ma et al. (2016) and Saul et al. (2019), which showed that the OTL flow at the rear of the rims is dominated by the pressure differentials and not the casing motion.

6.2 Sensitivity to Coolant Density

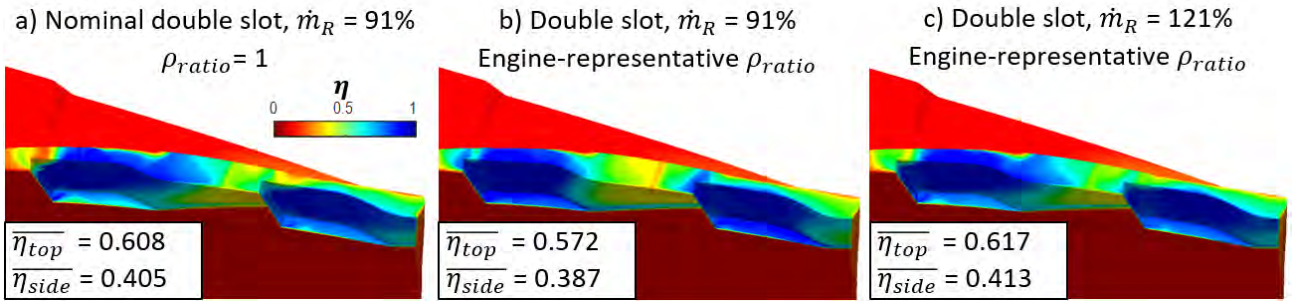

Figure 13: Film cooling effectiveness contours for the double slot geometry. On the left, nominal case discussed in Sections 4.5 and 5 with a total coolant mass ratio of 91% and coolant to mainstream density ratio of 1. On the middle, case with the same coolant mass flow rate but with an engine-representative density ratio. On the right, case with engine-representative density ratio and matching jet Mach number to that of the nominal condition. All three cases were simulated with a tip gap size of 1.15% g/S.

Figure 13 compares CFD predictions of the double slot design at the nominal coolant to mainstream density ratio, ρ_{ratio} = 1, to the same geometry at engine-representative density ratio, both matching coolant mass flow rate (middle plot) and matching the Mach numbers of the cooling jets (right plot). Data show that the cooling coverage is largely determined by the Mach number of the cooling jets. Matching coolant mass flow rate while keeping the geometry constant (13.a and 13.b) causes a decrease in effectiveness in line with a reduction of BR (see Figure 8). In contrast, the case with matching Mach numbers of the cooling jets exhibits near identical performance metrics to that of the nominal case (13.a and 13.c). For the same geometry, this required a mass flow rate increase of approximately 30%, but this could be mitigated by instead reducing slot flow area (l and d_n). The effectiveness at high density remains significantly better than conventional designs.

7 CONCLUSIONS

This paper has demonstrated the potential benefits of the inclined slot cooling concept for cooling blade tips. Numerical simulations explored the design space and the most promising geometry was experimentally validated in a cascade. The key conclusions are as follows:

- Both computations and experiments show that the dedicated inclined slot concept can greatly improve tip cooling on both the side and top of the critical pressure side rim of the tip.
- As per conventional cooling holes, the inclined slot performance is dependent on the blowing ratio. The behaviour

can be largely understood by considering the injected streamwise momentum. Low blowing ratios lead to higher coolant concentrations near the slot, but with little streamwise propagation. Conversely, higher blowing ratios cause the coolant to propagate over a longer distance, enhancing downstream coverage. However, coolant concentration in the near-slot region reduces due to enhanced mixing with the mainstream flow. For a balanced blowing ratio, the slot designs can achieve high levels of coolant coverage over a distance of around 20% C_{ax} downstream of the slot.

- Low slot ejection angles are optimal, as they improve the alignment of the coolant jets with the pressure side rims, enabling the jets to more easily propagate along the rim surfaces.
- The double slot configuration maximises coolant concentration and coverage. The two slots can be adjusted to work in tandem at their respective optimal ranges. This configuration achieved continuous high coolant density over the pressure side rim, greatly outperforming conventional cooling strategies.
- Experimental cascade data corroborated the numerical studies. Compared to conventional cooling design, the double slot geometry achieving an effectiveness improvement of 45% on the rim tips, whilst using 25% less coolant.
- Further computations show that the inclined slot design should have high performance in real turbine conditions. Relative casing motion has negligible impact on performance because the local over-tip flow is pressure dominated. Increasing coolant density reduces the injected momentum of the coolant jet, thus reducing its streamwise propagation; this effect can be mitigated by reducing the slot area to increase the injected velocity.

NOMENCLATURE

Abbreviations

BR	Blowing Ratio
dif	Difference
FCE	Film Cooling Effectiveness
HP	High-Pressure
LE	Leading Edge
OTL	Overtip Leakage
PS	Pressure Side
SS	Suction Side
TE	Trailing Edge

Symbols

A_i	Initial Area [m^2]
C_{ax}	Axial Chord [m]
d	Distance or Shelf Depth [m]
d_n	Slot Nominal Diameter [m]
g	Tip Gap [m]
h	Shelf bottom offset [m]
l	Slot Length [m]
L	Shelf Length [m]
$\dot{m}_R$	Non-dimensionalised Coolant Mass Flow Rate
S	Blade Span [m]
T	Temperature [K]
V	Velocity [m/s]
w	Shelf Width [m]
α	Shelf Inclination
β	Shelf Pitch
η	Film Cooling Effectiveness
ρ	Density [kg/m^3]

Subscripts

av	Area-Average
c	Coolant
g	Gas
m	Mainstream
$test$	Test or Baseline
top	Top Surface
ref	Reference
$side$	Side Surface
$wall$	Wall

ACKNOWLEDGMENTS

The authors would like to express gratitude to the Engineering and Physical Sciences Research Council, Innovate UK iCore project, Rolls-Royce and Aerospace Technology Institute for funding this project. In addition, thanks to the following for their contributions: Andrew Melzer for his help in the calibration of the aerodynamic probe; Rolls-Royce personnel for their technical assistance, particularly Eduardo Romero, Haidong Li and Paolo Valloni; and technicians at the Oxford Thermofluids Institute for their help with the facilities.

REFERENCES

Ahn, J., Mhetras, S. and Han, J. (2005), 'Film-cooling effectiveness on a gas turbine blade tip using pressure-sensitive paint', *J. of Turbomachinery* **127**. DOI: 10.1115/1.1909208.

Bunker, R. (2004), 'Blade tip heat transfer and cooling techniques.', *von Karman Institute for Fluid Dynamics, Lecture Series 2004* .

Cherry, D., Lee, C., Prakash, C., Wadia, A., Keith, B. and Brassfield, S. (2002), 'Turbine blade having angled squealer tip'. U.S. Patent 6,672,829.

Correia, V., Manning, R. and Reddy, B. (2008), 'Turbine blades and turbine blade cooling systems and methods'. U.S. Patent 20,080,131,278.

Crites, C., Morris, C. and Halfmann, S. (2013), 'Ep 2 639 405 a1'. EU Patent EP 2 639 405 A1.

Cunha, F. and Chyu, K. (2006), 'Trailing-edge cooling for gas turbines', *Journal of Propulsion and Power* **22**. DOI: 10.2514/1.20898.

Denton, J. (1993), 'Loss mechanisms in turbomachines', *J. of Turbomachinery* .

Dutta, S., Ekkad, S. and Han, J. (2000), *Gas Turbine Heat Transfer and Cooling Technology*, CRC Press, Florida.

Han, J. and Rallabandi, A. (2010), 'Turbine blade film cooling using PSP technique. frontiers in heat and mass transfer', *Frontiers in Heat and Mass Transfer* **130**. DOI: 10.1115/1.2776949.

Hofer, T. and Arts, T. (2009), 'Aerodynamic investigation of the tip leakage flow for blades with different tip squealer geometries at transonic conditions', *Proceedings of the ASME Turbo Expo* **7**. DOI: 10.1115/GT2009-59909.

Kwak, J. and Ahn, J. (2003), 'Heat transfer coefficients and film cooling effectiveness on the squealer tip of a gas turbine blade', *J. of Turbomachinery* **125**. DOI: 10.1115/1.1622712.

Lee, C., Brainch, G. and Isburgh, A. (1998), 'Slot cooled blade tip'. U.S. Patent 573,310,2 A.

Leeke, L., Keith, S., Rae, R., Lenahan, D., Harris, D. and Frey, D. (2003), 'Ramped tip shelf blade'. U.S. Patent 20,030,059,304.

Ma, H., Zhang, Q., He, L., Wang, Z. and Wang, L. (2016), 'Cooling injection effect on a transonic squealer tip: Part 1 — experimental heat transfer results and cfd validation', *Proceedings of the ASME Turbo Expo* **5A**. DOI: 10.1115/GT2016-57579.

Menter, F. (1994), 'Two-equation eddy-viscosity turbulence models for engineering applications', *AIAA Journal, No. 8* **32**. DOI: 10.2514/3.12149.

Moinier, P. (1999), Algorithm developments for an unstructured viscous flow solver, DPhil Thesis, PhD thesis, University of Oxford.

Niharika, G., Wong, T., Ireland, P. and Self, K. (2016), 'Study of film cooling in the trailing edge region of a turbine rotor blade in high speed flow using pressure sensitive paint', *Proceedings of ASME Turbo Expo 2016* **5C**. DOI: 10.1115/GT2016-57356.

O'Dowd, D., Zhang, Q., He, L., Cheong, B. and Tibbott, I. (2013), 'Aerothermal performance of a cooled winglet at engine representative mach and reynolds number', *J. of Turbomachinery* **135**. DOI: 10.1115/1.4006537.

Saul, A., Ireland, P., Coull, J., Wong, H., Li, H. and Romero, E. (2019), 'An experimental investigation of adiabatic film cooling effectiveness and heat transfer coefficient on a transonic squealer tip', *J. of Turbomachinery* **138**. DOI: 10.1115/1.4043263.

Vieira, J., Coull, J., Ireland, P. and Romero, E. (2021), 'Aerothermal effect of cavity welding beads on a transonic squealer tip', *J. of Turbomachinery* **143**. DOI: 10.1115/1.4051267.

Virdi, A., Zhang, Q., He, L., Li, H. and Hunsley, R. (2015), 'Aerothermal performance of shroudless turbine blade tips with relative casing movement effects', *Journal of Propulsion and Power* **31**. DOI: 10.2514/1.B35331.

Wong, T., Ireland, P. and Self, K. (2016), 'Film cooling effectiveness downstream of trailing edge slots including cutback surface protuberances', *Int. J. Turbomach. Propuls. Power* **1**. DOI: 10.3390/ijtpp1010004.

Yang, Z. and Hu, H. (2012), 'An experimental investigation on the trailing edge cooling of turbine blades', *Journal of Propulsion and Power* **1**. DOI: 10.1016/j.jppr.2012.10.007.

Zhang, B., Yao, C., Zhu, H., Liu, C. and Sunden, B. (2022), 'Experimental study on film cooling performance of a turbine blade tip with a trapezoidal slot cooling scheme in transonic flow using psp technique', *Experimental Thermal and Fluid Science* **130**. DOI: 10.1016/j.expthermflusci.2021.110513.

Zhang, B., Zhu, H., Yao, C. and Liu, C. (2021), 'Investigation on aerothermal performance of a rib-slot scheme on the multi-cavity tip of a gas turbine blade', *International Journal of Heat and Mass Transfer* **176**. DOI: 10.1016/j.ijheatmasstransfer.2021.121408.

Zhang, Q., O'Dowd, O., He, L., Wheeler, S., Ligrani, M. and Cheong, Y. (2011), 'Overtip shock wave structure and its impact on turbine blade tip heat transfer', *J. of Turbomachinery* **133**. DOI: 10.1115/1.4002949.